Dynamic Behavior of Fatty Acid Spin Labels within a Binding Site of Soybean Lipoxygenase-1[†]

Fayi Wu and Betty J. Gaffney*

Department of Biological Science, Florida State University, Tallahassee, Florida 32306-4370

Received July 13, 2006; Revised Manuscript Received August 18, 2006

ABSTRACT: The putative substrate-binding site in lipoxygenases is long and internal. There is little direct evidence about how the unsaturated fatty acid substrates enter and move within the cavity to position themselves correctly for electron transfer reactions with the catalytic non-heme iron. An EPR spectroscopy approach, with spin-labeled fatty acids, is taken here to investigate dynamic behavior of fatty acids bound to soybean lipoxygenase-1. The probes are labeled on C5, C8, C10, C12, and C16 of stearic acid. The EPR-determined affinity for the enzyme increases as the length of the alkyl end of the probe increases, with a $\Delta\Delta G$ of −190 cal/methylene. The probes in the series exhibit similar enhanced paramagnetic relaxation by the iron center. These results indicate that the members of the series have a common binding site. All of the bound probes undergo considerable local mobility. The stearate spin-labeled at C5 has the highest affinity for the lipoxygenase, and it is a competitive inhibitor, with a K_i of 9 μM. Surprisingly, this stearate labeled near the carboxyl end undergoes more local motion than those labeled in the middle of the chain, when it is bound. This shows that the carboxyl end of the fatty-acid spin label is not rigidly docked on the protein. During catalysis, repositioning of the substrate carboxyl on the protein surface may be coupled to motion of portions of the chain undergoing reaction.

Lipoxygenase (LOX)[1] enzymes catalyze the first step in one of the major pathways to molecules derived from arachidonic acid. A theme emerging from the medical perspective on different human lipoxygenases is one of positive and negative influences on human health from these molecules (*1*, *2*). Thus, there is much interest in being able to pharmaceutically modulate the activity of selected members of the lipoxygenase family while leaving other members functioning normally (*3*, *4*). Indeed, inhibitors selective for 5-, 12-, or 15-arachidonic acid lipoxygenases have been developed (*5*−*7*). Lipoxygenases from both plant and animal sources have overall structural similarity with a long internal cavity that passes by the catalytic iron ion, based on available X-ray structures (*8*−*14*). Some determinants of substrate binding within this cavity have been examined by mutation and modeling (*15*−*20*), but there is little direct experimental evidence about how fatty acids enter or interact with the cavity. In this report, we take a spectroscopic approach, with spin-labeled fatty acids, and examine the dynamic behavior of fatty acids bound to soybean lipoxygenase-1 (SBL1), the most studied representative of the family of LOX enzymes. SBL1 is a 13-linoleic acid, or 15-arachidonic acid, LOX.

The most detailed information available at present about substrate disposition within LOX cavities is based on enzyme kinetics and product analyses. The LOX mechanism (*21*) includes the enzyme with iron in two redox states (*22*). The rate-limiting step in the catalyzed reaction is stereoselective abstraction of a hydrogen atom, a proton-coupled electron transfer, from a bisallylic methylene of the substrate. This step is accompanied by reduction and protonation of the ferric−hydroxo metal center, involves hydrogen tunneling, and exhibits a large kinetic isotope effect (*23*). Subsequently, oxygen reacts with the delocalized radical intermediate at a position usually two carbons removed from the original site of hydrogen abstraction, giving a fatty acid peroxyl radical. Oxygen addition is usually *antara*-facial to the hydrogen that is removed, but there is an exception (*24*); in either case, it is highly stereoselective (*25*, *26*). Finally, the peroxyl radical accepts an electron from iron to return the metal center to the ferric−hydroxo form. The substrate cavity is very restricted as it passes iron, and a structural basis for the mechanism needs to describe the rearrangements that allow both of the electron transfer steps between fatty acid and metal to occur on effectively opposite sides of the substrate.

Placement of the substrate carboxyl has received much attention in proposals for the molecular basis of catalysis by lipoxygenases. There are two structures of molecular complexes with lipoxygenases that provide input about possible placement of the carboxyl. In the first of these, the carboxylate of an inhibitor (RS75091) is ∼3.8 Å from ferrous iron, close enough that it might become a ligand in the ferric enzyme form (*10*). In the second complex, the carboxylate

[†] This work was supported by NIH Grant GM65268 (B.J.G.).

* To whom correspondence should be addressed. Telephone: (850) 644-8547. Fax: (850) 644-0481. E-mail: gaffney@bio.fsu.edu.

[1] Abbreviations: cmc, critical micelle concentration; EPR, electron paramagnetic resonance; LOX, any lipoxygenase; SBL1, soybean lipoxygenase isoform-1; 13*S*-HPODE, 13(*S*)-hydroperoxyoctadecadienoic acid; cAOS, coral allene oxide synthase; 2,2-substituted-4,4-dimethyl-3-oxazolidinyloxy, 1-oxyl-2,2,5,5-tetramethyloxazolidinyl; *x*-DSA, doxyl stearic acid spin label with a doxyl ring on carbon *x*; TEMPOL, 1-oxyl-2,2,6,6-tetramethyl-4-piperidinol; $2A_{zz}$, rigid limit separation of outer extrema in spin-label EPR spectra; $2A_{||}'$, separation of outer extrema when motion is present; $P_{1/2}$, microwave power at which the EPR signal is half the value extrapolated from low power; CHES, 2-(cyclohexylamino)ethanesulfonic acid.

10.1021/bi061415l CCC: $33.50
Published on Web 09/20/2006

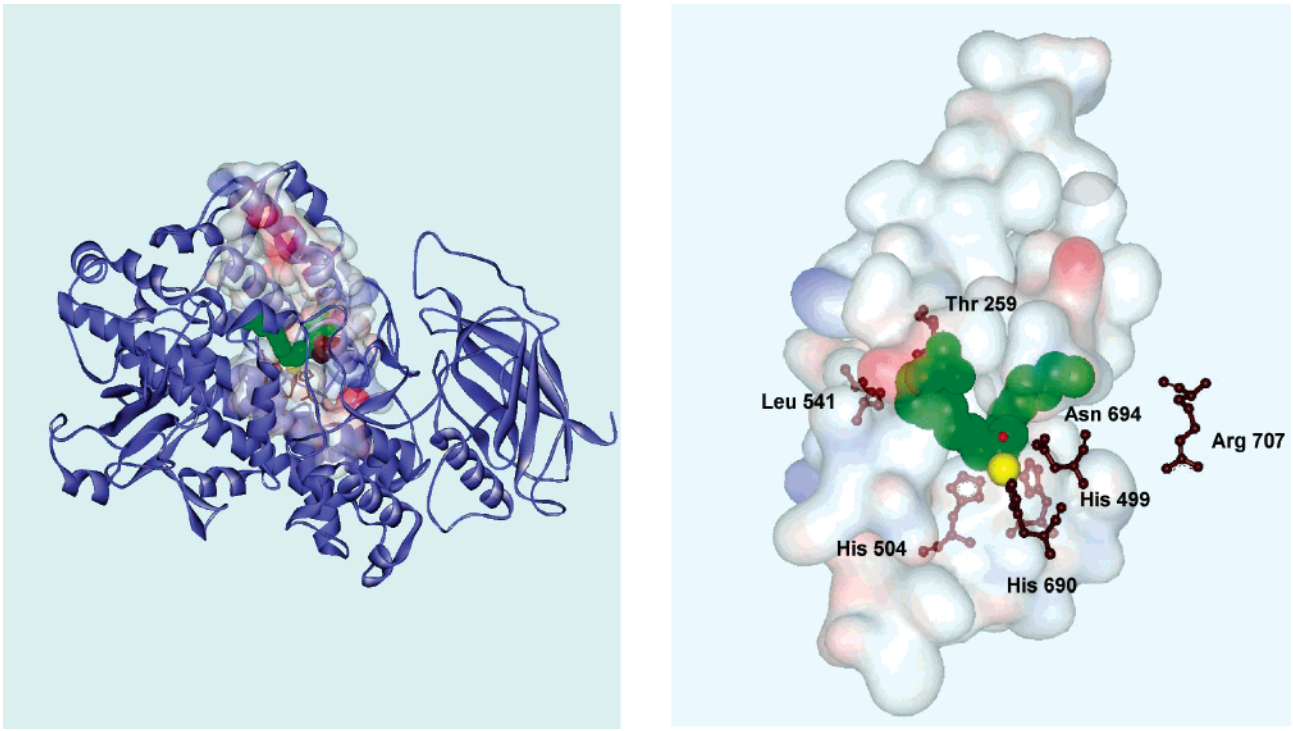

FIGURE 1: Structure of soybean lipoxygenase-1 and a region containing residues thought to influence substrate binding. The portion of the structure shown in detail (right) also appears as a shaded surface in the overall structure (left). The detailed structure portion is rotated from its position in the overall structure by an ~180° rotation about a vertical axis. This figure was rendered using coordinates of PDB entry 1YGE (*9*) and a Web Lab viewer demo (Accelrys, San Diego, CA). The docked linoleic acid (green) is from a model described in ref *20*. The catalytic iron is colored yellow, and the iron-bound water is represented as a red sphere. A possible entrance to the substrate cavity is flanked by Thr259 and Leu541 (*9*). Four of the protein side chains that are iron ligands are highlighted in brown. The remaining iron ligand, Ile839 carboxylate, is above the represented plane and is not shown. In the right panel, the red surface close to Thr259 and Leu541 is the negative charge of Glu256, and the other red surface is Glu752. The blue surfaces are positive charges [Lys260 (higher) and Arg543 (lower) in the right panel].

of the product and activator, 13(*S*)-hydroperoxyoctadecadienoic acid (13*S*-HPODE), lies deeply in the internal cavity of the soybean LOX isoform, SBL3, and there it interacts with Arg726 (equivalent to Arg707 in SBL1) (*12*). The peroxidate is a ligand to ferric iron in this structure. Models of LOX-bound substrate with similar carboxyl placements have been proposed (*12*, *19*, *27*, *28*). On the other hand, lipoxygenases are also reactive with esters of fatty acid substrates (*15*, *29*), and these substrates are not expected to coordinate iron or form ionic interaction with a buried arginine. A different category of model places the polar end of the substrate near the protein surface, close to one suggested entrance to the cavity in SBL1 between Thr259 and Leu541 (*9*). In this arrangement, the hydrophobic end of the substrate lies deeply in the binding pocket (*18*, *20*), as shown in Figure 1, essentially in an orientation that is the reverse of that of the product in the purple lipoxygenase structure (*12*). In fact, the stereochemistry of products from double dioxygenations of arachidonic acid demonstrates that substrates can be positioned correctly for catalysis in two orientations: with the methyl end of the substrate chain entering the cavity most deeply or, alternatively, with the carboxyl end entering most deeply (*20*). The former is preferred for the single dioxygenation reactions. The dual orientation option may help explain mixed modes of enzyme inhibition by substrate analogues (*30*).

A major hydrophobic contribution to binding is apparent from experiments with LOX substrate analogues. Highly specific inhibitors of rabbit 15-LOX [RS75091, $K_i = 3\ \mu M$ (*10*)] and leukocyte 12-LOX [varied structures with K_i values from 0.035 to $>2\ \mu M$ (*5*)] are substrate-length molecules with selectively placed aromatic rings and alkynyl groups. In other studies, it is shown that the effectiveness of *n*-alcohols of 2−12 carbons, or related molecules with alkyl chains similar in length, as weak inhibitors of SBL1 increases with chain length, to ~10 carbons (*31*−*33*).

To bridge the gap between X-ray structures and modeling, we take a spectroscopic approach to establish determinants of binding of fatty acids to SBL1 with a series of spin labels, doxyl stearic acids, DSAs (*34*). For comparison, interactions of the DSA probes with a different iron-containing enzyme that converts lipoxygenase products, coral allene oxide synthase (cAOS) (*35*), were examined also. Spin labels are versatile in the ways they can be applied. We examine electron paramagnetic resonance (EPR) spectra here to map the affinity of the series of DSA molecules for SBL1, to detect the proximity of DSA spin and iron, and to evaluate motion of the probes within the binding site. We find that a stearate labeled near the carboxyl is more mobile in the binding site than other members of the series labeled nearer the middle of the fatty acid chain, and all probes undergo some motion within the binding site.

MATERIALS AND METHODS

Spin-labeled (doxyl) stearic acids (DSAs) were obtained from Avanti Polar Lipids (Alabaster, AL) or were available locally from synthesis (*34*). The spin label 1-oxyl-2,2,6,6-

tetramethyl-4-piperidinol (TEMPOL, both ^{14}N and ^{15}N derivatives) was prepared locally as described previously (*34*). Soybean lipoxygenase-1 was purified as described previously (*36*) except the anion exchange medium was DE53 (Whatman) and a high-pressure liquid chromatography step was omitted. Expression and purification of C-terminally His-tagged cAOS were as described previously (*37*). Data fits were performed using fitting options available in KaleidaGraph (Synergy.com) and appropriate equations or, in the case of kinetics, VisualEnzymics (Softzymics.com).

Solubility of Spin-Labeled Fatty Acids

The solubilities of DSA molecules were determined using serial dilutions of each label in working buffer, and the intensity of the sharp three-line EPR spectrum was monitored. All of the DSA spin labels were soluble in 2 mM sodium hydroxide, and stock solutions prepared in this way were stored in plastic. Concentrations of the stock solutions were determined by comparison of double integrals of EPR spectra of the stock DSA solution and a solution of accurately weighed TEMPOL. Stock DSA solutions were diluted into 0.1 M CHES (pH 10) to the desired concentration. Further 1:1 dilution of the DSA solution with 0.2 M Tris (pH 8.35) gave final solutions for solubility determination by EPR in 0.1 M Tris and 0.05 M CHES (pH 8.4). The stearate spin labels that were examined were the 5-, 8-, 10-, 12-, and 16-doxyl derivatives. The maximal solubility of each label, the cmc, is taken as the highest concentration at which the EPR signal intensity as a function of label concentration is linear. The estimated values of cmc (millimolar) at pH 8.4 determined in this manner are 0.03 (5-DSA), 0.09 (8-DSA), 0.2 (10-DSA), 0.4 (12-DSA), and 0.1 (16-DSA). These values are given as estimates because substantial errors were encountered in making accurate dilutions of DSA molecules over a wide concentration range, presumably because fatty acids have some affinity for all surfaces (*38*).

Determination of Dissociation Constants

The dissociation constant, K_d, for dissociation of different DSA spin labels from SBL1 was determined using a constant DSA concentration and variable protein concentrations. The relative concentrations of free ^{14}N-labeled DSA were determined in each protein-containing sample by comparison with the amplitude of the same ^{14}N-labeled DSA in buffer without protein. The real concentration of the solution of each ^{14}N-labeled DSA in buffer without protein was determined by comparison of double integrals with double integrals of a solution of accurately weighed ^{14}N-labeled TEMPOL. An internal standard of ^{15}N-labeled TEMPOL was included in titration samples as a convenience in determining relative concentrations of free ^{14}N-labeled DSA with varied amounts of SBL1. Protein, spin label, and the standard were mixed immediately before each measurement. EPR signal amplitudes did not decrease within the preparation and recording time (<30 min). The concentration of bound DSA was taken as the concentration of total DSA minus the concentration of free DSA. At each protein concentration, three measurements were taken. The data were fit to the equation: fraction bound $= [P]/(K_d + [P])$, where [P] is the protein concentration at each point.

EPR Spectroscopy

Instrumentation. X-Band EPR spectra were obtained with a Varian E109 spectrometer equipped with an Oxford Instruments pumped, liquid helium flow cryostat. All low-temperature samples, in sealed 50 μL glass microcapillaries, were held in X-band quartz EPR tubes (4 mm outside diameter) containing 99% glycerol, for temperature stability. At X-band, the microwave frequency when the outer tube contained glycerol was 9.2594 ± 0.0001 GHz. Samples for room temperature (295 K) EPR were in 50 μL capillaries held in an outer, 4 mm quartz EPR tube filled with air. In this case, the frequency was 9.2613 ± 0.0001 GHz. Other parameters of X-band recording are specified in figure legends and table footnotes.

Samples. Samples were prepared either in 0.1 M Tris and 0.05 M CHES (pH 8.4) or in 0.1 M Tris and 0.05 M borate (pH 8.7) (see the figure legends). Glycerol was not added to samples unless specified.

Progressive Power Saturation. The peak-to-peak amplitude of the center line (corresponding to nitrogen nuclear spin $m_I = 0$) in the EPR spectra of DSAs bound to either SBL1 or cAOS was recorded for varied microwave powers. Separate power-saturation experiments were examined with samples at temperatures of 20, 40, 60, 80, 100, and 120 K. The power-saturation samples were prepared as described above, at pH 8.4, but glycerol was added to a final concentration of 25%. The value of $P_{1/2}$ was determined by fitting data acquired from 0.01 to 100 mW to eq 1, allowing b to float in determining the best fit (*39*).

$$\frac{I}{\sqrt{P}} = \frac{K}{\left(1 + \frac{P}{P_{1/2}}\right)^{b/2}} \quad (1)$$

In eq 1, P is the incident power, $P_{1/2}$ is the power at which the signal intensity is half the value predicted from linear behavior at low power, and K is a constant.

Enzyme Kinetics

Kinetic experiments were performed on a Cary 50 UV−vis spectrophotometer with an RX 2000 stopped-flow mixing accessory (Applied Photophysics). One syringe contained substrate and DSA at varied concentrations in 0.1 M sodium borate (pH 10). The other syringe contained 35 nM SBL1 in the same buffer. Equal volumes were mixed. The SBL1 solutions were made up immediately before each run from a 30 μM stock solution in 10 mM sodium acetate (pH 4.6). Data from the first two shots were discarded, and the results of the next three were averaged. The reaction rates were measured at the maximum of the reaction progress curve. Under these conditions, the maximal rate was obtained in 1.5−3 s.

RESULTS

Restricted Motions of Spin-Labeled Stearates Bound to SBL1. All of the stearate spin labels (DSAs) that were examined gave EPR signals indicating some degree of immobilization upon incubation with lipoxygenase (Figure 2). The ratio of DSA to protein (0.25) was chosen to minimize interaction with weak binding sites, if any. The

Table 1: Separation of Outer Extrema in the EPR Spectra of Spin-Labeled Stearates Bound to Lipoxygenase and Coral Allene Oxide Synthase[a]

	$2A_{zz}$ for SBL1 at 100 K (mT)	$2A_{\|\|}'$ for SBL1 at 295 K	$A_{\|\|}'/A_{zz}$ for SBL1 at 295 K	$2A_{zz}$ for cAOS at 100 K (mT)	$2A_{\|\|}'$ for cAOS at 295 K	$A_{\|\|}'/A_{zz}$ for cAOS at 295 K
5-DSA	7.09	5.99	0.84	7.01	5.39	0.77
8-DSA	7.00	6.17	0.88	7.04	6.07	0.86
10-DSA	7.01	6.20	0.88	6.87	6.27	0.91
12-DSA	6.86	6.18	0.90	6.96	6.18	0.89
16-DSA	6.95			7.03		

[a] Proteins (1.1 mM) and spin labels (0.25 mM) are in 0.05 M CHES and 0.1 M Tris (pH 8.4). The estimated error in values of $2A_{zz}$ or $2A_{\|\|}'$ is $\pm$0.02 mT. A value of $2A_{\|\|}'$ could not be determined for 16-DSA.

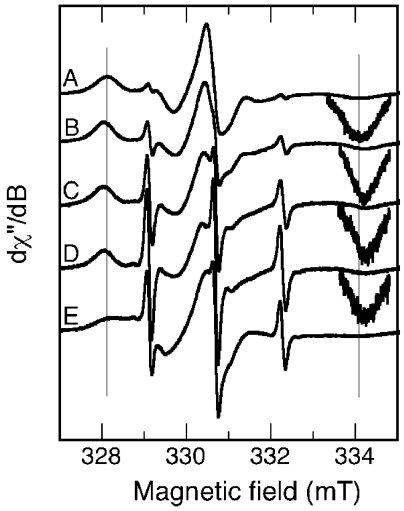

FIGURE 2: EPR spectra of soybean lipoxygenase-1 with a series of spin-labeled (doxyl) stearic acids. The EPR spectra show that there are differences in motional freedom and the affinity of different stearic acid spin labels, DSAs (0.25 mM), bound to soybean lipoxygenase-1 (SBL1, 1.1 mM, pH 8.4). Broad features in the EPR spectra are caused by bound spin labels; sharp peaks are caused by unbound spin labels. The DSA molecules giving each spectrum are labeled by the carbon number bearing the spin-label ring: (A) 5-DSA, (B) 8-DSA, (C) 10-DSA, (D) 12-DSA, and (E) 16-DSA. The vertical lines highlight the differences of outer extrema in the various spectra; the lines are drawn at the magnetic fields of the outer extrema for 5-DSA. EPR spectra were recorded at 295 K with a modulation amplitude of 0.1 mT and a power of 5 mW.

degree of immobilization, reflected in the separation of low-field maxima and high-field minima in the spectra ($2A_{\|}'$), varied. The vertical lines drawn in Figure 2 are at the magnetic fields of the low- and high-field extrema in the EPR spectrum of bound 5-DSA. The separation of these extrema, shown in Figure 2 for the 5-DSA spectrum, is called $2A_{\|}'$. The value of $2A_{\|}'$ from the spectra of bound 8-, 10-, and 12-DSA labels is larger than that for the 5-DSA spectrum (larger separation of outer extrema). The range of values of $2A_{\|}'$ for the spectra shown in Figure 2 is from 6.00 to 6.36 mT (Table 1). An entry for the EPR spectrum of 16-DSA is not included in Table 1 because a unique separation, $2A_{\|}'$, cannot be distinguished. The entries for cAOS are addressed later.

Samples prepared in the same manner as those in Figure 2 were also examined in the frozen state to determine the rigid limit values of the outer splittings, $2A_{zz}$. There are small differences among the DSA molecules bound to SBL1 in the rigid limit $2A_{zz}$ value, with 5-DSA having the largest (7.08 mT) and 12-DSA the smallest (6.88 mT) values. These differences suggest that the polarity of the immediate environment of the DSA molecules decreases in the following order: 5-DSA > 8-DSA $\approx$ 10-DSA > 16-DSA > 12-DSA. Using the ratio $A_{\|}'/A_{zz}$, also given in Table 1, allows the effects of motional averaging on different room-temperature spectra to be compared in a polarity-free manner. In the absence of motion, the ratio is 1.

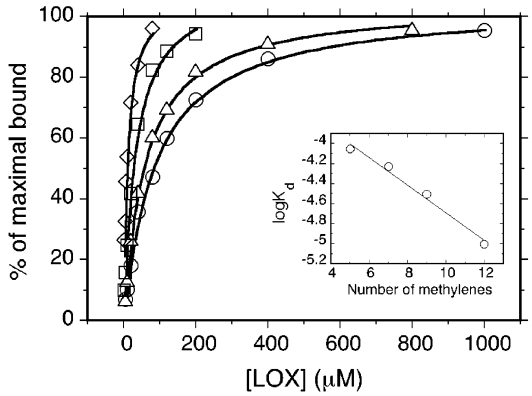

FIGURE 3: Binding of DSA spin labels as a function of SBL1 concentration. A constant concentration of DSA was titrated with variable concentrations of SBL1 (pH 8.7): (◇) 16 μM 5-DSA, (□) 24 μM 8-DSA, (△) 23 μM 10-DSA, and (○) 22 μM 12-DSA. In the inset, values of log K_d are plotted as a function of the number of methylenes between the carbon bearing the spin label and the methyl end of the stearate chain. Data are derived from EPR spectra recorded at X-band (295 K) with a microwave power of 5 mW and a modulation amplitude of 0.125 mT.

Table 2: Affinities of DSA Spin Labels Bound to SBL1[a]

	K_d (μM)	log(K_d)		K_d (μM)	log(K_d)
5-DSA	10 ± 1	-5.0	10-DSA	59 ± 2	-4.2
8-DSA	31 ± 2	-4.5	12-DSA	88 ± 5	-4.1

[a] The DSA concentration was held constant, and the SBL1 concentration was varied. The DSA concentrations were 16 μM for 5-DSA, 24 μM for 8-DSA, 23 μM for 10-DSA, and 22 μM for 12-DSA. The K_d values and errors were determined by fits to experimental data (Figure 3) as outlined in Materials and Methods.

Hydrophobic Interactions of Spin-Labeled Stearates with SBL1. Inspection of Figure 2 reveals that, in the EPR spectra of DSAs labeled on C5, C8, C10, and C12, the intensity of the sharp signals from unbound DSA increases as the number of methylenes between the carbon bearing the label and the terminal methyl decreases. 16-DSA is an exception to this trend and probably has a mode of binding different from those of the rest of the series. Dilution of samples giving the spectra in Figure 2 gave new EPR spectra in which the fraction of free signal was increased, indicating that the free and bound spin labels are in reversible equilibrium. A fixed concentration of 5-, 8-, 10-, or 12-DSA was titrated with SBL1 to determine the values of the dissociation constants, K_d (Figure 3 and Table 2). We found less scatter in the binding data when titrations were performed with a constant DSA concentration (variable protein concentration) rather

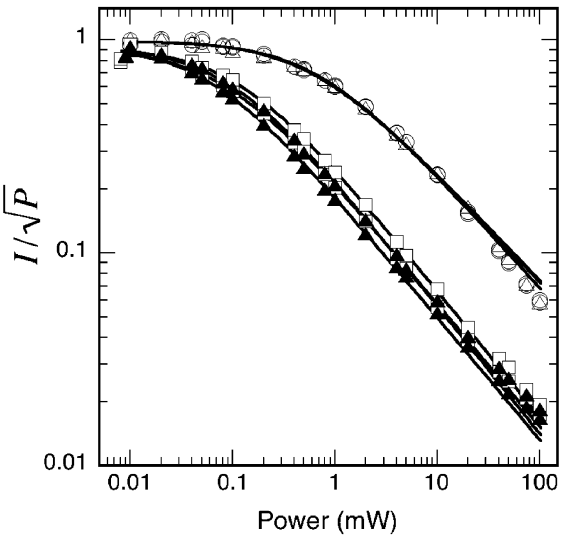

FIGURE 4: Progressive power saturation of 5-DSA with several proteins. The EPR spectra of 5-DSA bound to two paramagnetic proteins, SBL1 (○) and cAOS (△), to the diamagnetic protein bovine serum albumin, BSA (□), and to the spin label TEMPOL in the presence of SBL1 (▲) were examined by progressive power saturation at 60 K. Protein concentrations were 0.63 mM (pH 8.4); two determinations each were made for SBL1, BSA, and TEMPOL/SBL1, and one determination was made for cAOS. The molar ratios of 5-DSA to proteins were 0.3 for SBL1 and BSA, 0.17 for cAOS, and 0.4 for TEMPOL/SBL1. EPR spectra were recorded with a modulation amplitude of 0.4 mT. The lines shown are the curve fits from eq 1.

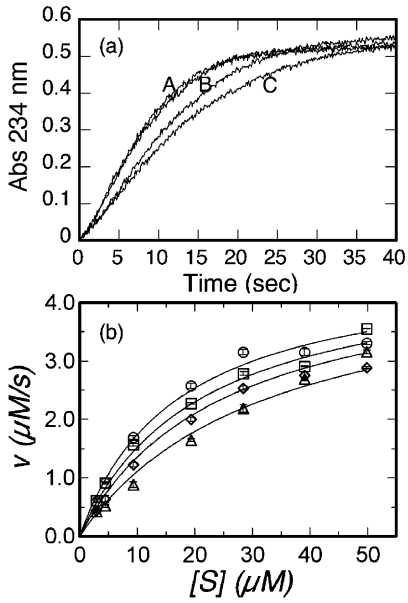

FIGURE 5: (a) Reaction progress of SBL1 with linoleic acid in the presence or absence of 5-DSA. The substrate (20 μM) reacted with 17.5 nM SBL1 [0.1 M sodium borate (pH 10)] in the absence or presence of 20 μM TEMPOL (A) or the presence of 4 (B) and 8 μM 5-DSA (C). (b) Computer fits of kinetics data to a competitive inhibition model for the reaction of SBL1 (17.5 nM) with linoleic acid in the absence (○) or presence of 5-DSA [2 (□), 4 (◇), and 8 μM (△)].

than with a constant protein concentration (variable DSA concentration), presumably because fatty acids have some affinity for surfaces used in aliquoting (*38*). Because different constant total spin-label concentrations were used in the various titrations, the combined data in Figure 3 are expressed in terms of the percentage of total label bound so that the four curves can be compared readily. The inset in Figure 3 is a plot of log(K_d) versus the number of CH_2 groups between the carbon bearing the doxyl ring and the methyl end of the molecule for the series from 5- to 12-DSA. The best fit to the points is the line shown, with the slope log(K_d)/methylene equal to −0.14 or a $\Delta\Delta G$ of −190 cal/methylene beyond the position of the doxyl ring.

Relaxation of the Doxyl Spin by Iron. Native lipoxygenase contains high-spin ferrous iron. Increased relaxation rates are expected if a spin label bound to a protein is close to a fast relaxer, such as iron. Continuous-wave EPR power saturation curves of 5-DSA bound to SBL1, of a water-soluble spin label in the presence of SBL1, and of BSA as a nonparamagnetic control were determined by EPR over the range of 20−120 K, and the 60 K data are given in Figure 4. Saturation data for another high-spin ferric enzyme with a fatty acid substrate, cAOS, are also shown. Values of $P_{1/2}$ were determined by curve fits (Materials and Methods). The value of $P_{1/2}$ is higher for the iron-containing proteins than for BSA at all temperatures, as expected. At 60 K, the $P_{1/2}$ value determined for 5-DSA bound to SBL1 is 0.61 mW and that for BSA is 0.10 mW; the $P_{1/2}$ value for cAOS is 0.57 mW, and for comparison, $P_{1/2}$ is 0.07 mW for the spin label TEMPOL in a solution of SBL1. At 100 K, the $P_{1/2}$ values were 3 times larger for the paramagnetic proteins than for BSA. At 20 K, the difference was ∼1 order of magnitude. The values of the exponent b in the curve fits varied from 1.0 to 1.2, and the errors in $P_{1/2}$ are ∼10% (eq 1). Saturation of other DSA molecules, 8-, 10-, and 16-DSA, by SBL1 iron was also examined at 100 K (data not shown). Significant differences between $P_{1/2}$ values of the DSA molecules were not observed.

Another test of the proximity of the spin label and iron is to determine if dipolar splitting is observed in very low-temperature EPR spectra (*40*). EPR spectra of 5-, 12-, and 16-DSA were examined in the temperature range of 5−20 K. Some line broadening was observed at the lowest temperature, but no resolved splitting was seen.

Spin-Labeled Stearates as Inhibitors of Lipoxygenase. Inhibition, by 5-DSA, of SBL1 oxidation of linoleic acid was examined at pH 10 (0.1 M sodium borate), using substrate and spin-label solutions without detergents. Figure 5 shows representative reaction progress curves, and a computer fit to data, for reactions of SBL1 with linoleic acid in the presence and absence of 5-DSA. The data shown in Figure 5b were obtained from kinetic traces (three each) with 0, 2, 4, and 8 μM 5-DSA and a 16.7-fold concentration (3−50 μM) range of linoleic acid, using 17.5 nM SBL1. The available range of 5-DSA concentrations was limited by the solubilities of the mixed fatty acids, and rigorous proof of a mode of inhibition could not be obtained. As an example, the data in Figure 5 are fit to a competitive model which, compared to an uncompetitive model, produces a slightly better fit (χ^2 is 0.48 and 1.09 for competitive and uncompetitive models, respectively). The parameters of the best fits to the two models are as follows: for the competitive model $V_{max} = 4.7 \pm 0.2$ μM/s, $K_m = 17 \pm 2$ μM, and $K_i = 9 \pm 1.5$ μM and, for the uncompetitive model, $V_{max} = 5.4 \pm 0.4$ μM/s, $K_m = 26 \pm 4$ μM, and $K_i = 18 \pm 5$ μM. The other DSA molecules were also examined by kinetics, but significant inhibition was not observed.

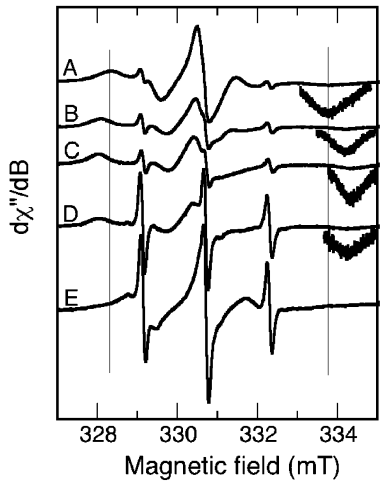

FIGURE 6: EPR spectra of cAOS with a series of spin-labeled stearic acids. This series of spectra for cAOS (1.1 mM) was obtained under conditions identical to those given in the legend of Figure 2. Different DSA molecules (0.25 mM), labeled by the carbon number bearing the spin-label ring, are (A) 5-DSA, (B) 8-DSA, (C) 10-DSA, (D) 12-DSA, and (E) 16-DSA.

In control experiments, kinetics curves were obtained with and without 1 mM TEMPOL added to linoleic acid (5−80 μM). The kinetics parameters were the same, so it is unlikely that free-radical reactions with a nitroxide are the source of inhibition by the DSA spin label. Although there is some leakage of substrate radicals from reactive intermediates in the lipoxygenase reaction (*41*), the EPR signal of 5-DSA (20 μM) is not reduced within 5 min when linoleate (40 μM) and SBL1 (17.5 nM) are combined.

Spin-Labeled Stearates Bound to Coral AOS. The dynamics and affinity of the DSA spin labels with cAOS were surveyed also (Figure 6), for comparison with the study of the affinity of these spin labels for SBL1. Differential motion of stearate chains labeled at various positions is even more pronounced in the case of cAOS compared to SBL1. The range of $2A_{||}'$ (295 K) is 5.40−6.19 mT for the various labels bound to cAOS. The corresponding values of $2A_{||}'/2A_{zz}$ for 5- and 10-DSA are 0.77 and 0.91, respectively (Table 1). As with SBL1 binding, the mobility of the bound spin label is greatest when the doxyl group is at either end of the chain. However, the affinity pattern through the series was different from the regular changes with alkyl chain length observed in binding of DSA to SBL1. Stearates 5- to 10-DSA had uniformly high affinity, and 12- and 16-DSA affinities were reduced.

DISCUSSION

A somewhat counterintuitive picture emerges from this spectroscopic study of binding of fatty acids to the 13/15-lipoxygenase, SBL1: a trend toward lower affinity correlates with stronger immobilization of the bound probe in a series of doxyl stearic acids, from 5- to 12-DSAs. Stearate chains labeled on C8 to C12 are immobilized to a greater extent than when the doxl group is on C5, but 5-DSA has the highest affinity (Tables 1 and 2). For this to be remarkable, it must be shown that the binding sites for the probes overlap. After a paragraph in which the degree of motion is evaluated, the ensuing paragraphs discuss the evidence pointing to a common binding site. At the outset, it is also noted that the affinity of 16-DSA is higher than expected by extrapolation from results with other members of the series and the motional freedom of this probe is unusually high. Data for 16-DSA are best interpreted in terms of a mode of binding different from those of the other DSAs.

The 5- to 16-DSA molecules examined here clearly undergo some local motion in their binding sites on SBL1, in addition to reflecting the overall tumbling of the protein. A qualitative measure of motion is obtained by comparing the ratio, $2A_{||}'/2A_{zz}$, of separation of the outer extrema in the EPR spectra of bound molecules for samples in solution and in frozen (rigid limit) forms (Table 1). The rotational correlation time for a hydrated spherical protein with the molecular mass of SBL1 (94 kDa), in aqueous buffer at 293 K, is approximately ∼39 ns [molecular mass/2.4 ps (*42*)]. The lipoxygenase structure has an axial ratio more like 2:1. The effects of diffusional anisotropy limit quantitative analysis of motion because the relation of the probe molecular principal axes to the diffusion axes is not known. However, a calculation appropriate for isotropic diffusion can be taken as a point of reference. The spin-label EPR ratio $A_{||}'/A_{zz}$ and the rotational correlation time τ_R, taking a commonly used Brownian diffusion model of spherical protein motion, are related by eq 2 (*43*, *44*).

$$\tau_R = (0.54\ \text{ns})\left(1 - \frac{A_{||}'}{A_{zz}}\right)^{-1.36} \qquad (2)$$

The ratio $A_{||}'/A_{zz}$ varies from 0.84 to 0.90 in the 5- to 12-DSA series, corresponding to rotational correlation times, from eq 2, of 6.5 ns (5-DSA) to 12.4 ns (12-DSA). Clearly, even considering SBL1 molecular anisotropy, each of the DSA molecules bound to SBL1 undergoes some local motion, in addition to reflecting overall protein diffusion, and 5-DSA is most mobile within its site, of the 5- to 12-DSA molecules. For comparison with the SBL1 data, the predicted (as described above) and EPR-determined [pH 7.0 (*45*)] rotational correlation times of 12-DSA bound to BSA are ∼28 and 30 ns, respectively. A further comparison can be made with 10-DSA bound to cAOS (43 kDa), for which the $A_{||}'/A_{zz}$ value is 0.91 and the EPR-determined and predicted correlation times are 14 and 18 ns, respectively. These comparisons emphasize the evident motion of the DSA probes in the binding site on SBL1.

Although the nitroxide rings sense differences in nearby polarity, two forms of evidence point to a common overall binding site for the 5- to 12-DSA series. First, the EPR-derived K_d values vary in a regular way in this series, with a common free energy per methylene on the methyl side of the spin-label ring ($\Delta\Delta G$) of approximately −190 cal/methylene. Second, progressive power saturation, which is related to the distance between the nitroxide and the fast-relaxing iron, is essentially the same for all the DSA molecules. A working model consistent with these data is shown in Figure 7. The model gives a representation of a binding site on SBL1, and the region shown would correspond to a small region of the whole protein. In the model, the doxyl rings of 8-, 10-, and 12-DSA are lodged at the entrance to a restricted cavity that leads to iron. The enhanced mobility in the binding site for 5- and 16-DSA molecules suggests that the hydrocarbon regions of 5- and 16-DSA are too long to move completely into the binding site and

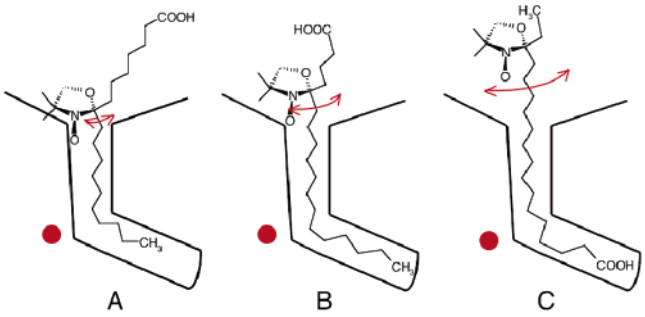

FIGURE 7: Working model of different DSA molecules bound to a channel in SBL1. (A) Stearates labeled in the middle of the chain (8-, 10-, and 12-DSA) have the least motion evident from EPR spectra, and they are proposed to lodge near the restricted cavity entrance. (B) 5-DSA has more motional freedom but is nearly the same distance from iron. (C) 16-DSA exhibits considerable motion and a polar environment. It is shown inverted in the channel compared to the other DSA molecules in panels A and B. Iron is shown as a red circle; red arrows signify the amplitudes of restricted motion.

fluctuate around the entry. To explain why 16-DSA does not follow the trend in K_d exhibited by the others and why the spin undergoes considerably more motion, the molecular orientation of 16-DSA in the binding site is proposed to be the opposite of that of the other DSA molecules. Since 12-DSA does not appear to adopt the same orientation as 16-DSA, it may be that the carboxyl of 16-DSA is deep enough in a cavity to form an ionic interaction that would not be available to the shorter carboxyl end of 12-DSA. These considerations raise the possibility that the 16-DSA carboxyl forms a charge interaction with iron. However, a binding site for 16-DSA that is completely different from that occupied by the other DSAs cannot be ruled out.

No dipolar split features were apparent in EPR spectra of DSA labels bound to SBL1 at very low temperatures (5−10 K) (*40*). The iron in resting SBL1 is high-spin ferrous iron ($S = 2$) and thus expected to have a zero field splitting (zfs) large compared to the X-band EPR energy. The expectation is that fast relaxation of the metal spin will be dominated by separation of ground and excited states, or by an Orbach process, in the temperature range from ~5 to 100 K, as it is for high-spin ferric iron with large zfs (*46*). In high-spin, spin-labeled porphyrins ($S = {}^5/_2$) that also have large zfs, a distance between nitroxide and iron of 11−15 Å resulted in resolved dipolar splitting in cw EPR spectra in the temperature range of 6−8 K (*40*). This would seem to rule out the possibility that 5-DSA is able to bind with the carboxyl deep in the SBL1 cavity because that location would place the nitroxide very close to iron. Progressive saturation at 60 K of 5-DSA gave a ratio of $P_{1/2}$ values of >8 for the probe on SBL1 compared to TEMPOL in an SBL1 solution, but not bound. Additionally, the half-saturation values measured at 100 K for 5-, 8-, 10-, and 16-DSA bound to SBL1 are identical, within the limits of this kind of measurement. Relaxation of radicals by ferrous iron in photosystems provides examples that can be used to estimate an upper bound to the distance of the DSA spins from ferrous iron in SBL1 (*39*). The ratio of $P_{1/2}$ with and without a relaxation contribution from iron, at 30 K, is ~8 for the primary acceptor, pheophytin, in photosystem II (*47*). This radical is 20 ± 4 Å from iron (*47*). The relaxation mechanism for the DSA spin labels on SBL1 has not been examined in detail yet, and the radicals in the two systems may have different inherent T_1 values; however, it is reasonable to suggest that the spin of 5-DSA is a distance from the SBL1 iron that is similar to the pheophytin−iron distance in PSII. Such a distance is compatible with the spin-label ring being positioned near the putative cavity entrance between Thr259 and Leu541; for instance, the distance from iron to Leu541 Cβ is 11.5 Å and to Ser261 Oγ is 18 Å.

The K_d of 5-DSA with ferrous SBL1, determined by EPR, is ~10 μM, while the K_m for linoleate substrate is ~15 μM, suggesting that 5-DSA might be effective as an inhibitor. Indeed, 5-DSA inhibited SBL1-catalyzed oxidation of linoleic acid with a K_i of 9.0 ± 1.5 μM. The values of K_d and K_i need not be the same, and since the primary form of the enzyme under turnover conditions is ferric, this K_i is a measure of the affinity of DSA molecules for ferric lipoxygenase while the EPR-determined binding curve (Figure 2) is for ferrous SBL1. There is precedent for an inhibitor having different affinities for ferrous and ferric 12-lipoxygenase (*30*). The inhibitor in that case has a K_i for ferrous 12-lipoxygenase of 0.07 μM and for the ferric enzyme of 2−4 μM. The other DSA molecules in the series did not significantly inhibit SBL1 turnover. Overall, the inhibition by 5-DSA suggests that some part of the substrate-binding site is the binding site for this spin label.

Interactions of the spin-labeled fatty acids with coral allene oxide synthase, cAOS (*35*), were examined for comparison with data from SBL1. The substrate of cAOS is the hydroperoxide product formed by its partner 8*R*-LOX. The substrate cavity in cAOS is U-shaped, and the distance from the surface to the heme iron, ~13 Å, would place the C8 OOH group of the substrate in position to react with the heme (*34*). The affinity pattern of the DSA series is different for cAOS and SBL1 (Figure 6). DSA molecules with alkyl chains of 8 to 12 carbons (5- to 10-DSA) had roughly equivalent affinities for cAOS. However, there are striking differences in motion of the various DSAs when they are bound. The difference in motion exhibited for 5-DSA compared to 8- and 10-DSA is even larger than it was for this comparison in SBL1 data. With regard to the distance of the DSA spin from iron, the half-saturation value of 5-DSA, relaxed by cAOS ferric iron at 60 K, is essentially the same as that value for relaxation of 5-DSA by SBL1 ferrous iron (Figure 4).

There is some information about sites where molecules dock from structures of lipoxygenases. An analogous region is involved in binding the inhibitors RS75091 to reticulocyte lipoxygenase (*10*) and epigallocatechin to the soybean LOX isoform, SBL3 (*48*). With regard to the helices of SBL1, this region begins between helices 2 and 11 and extends over the side of metal-binding helix 9 where water is coordinated to iron. Six to eight methylenes can be modeled in a hydrophobic cavity lying between iron and residues on helix 11, Ile538 or Leu541 (*18*, *20*). This hydrophobic region, between the surface and iron, is a likely site for binding of an aliphatic chain. In the case of the doxyl stearates, the spin-label ring is probably too bulky to pass through a restricted cavity entrance, an example of which might be between Thr259 and Leu541 (*9*). Thus, for each DSA in the series, increasing numbers of methylenes, those between the carboxyl and the spin-label ring, are exposed on the surface as the hydrophobic end of the stearate probe becomes shorter.

The net free energy per methylene for binding the hydrophobic end of a DSA molecule, approximately −190 cal/methylene, is smaller than typical values (approximately −600−800 cal/methylene) obtained when fatty acids of different total lengths are examined in binding to BSA or other proteins (*49*). Thus, there must be an unfavorable binding contribution from the portion of the DSA chain that remains on the surface of SBL1. A series of synthetic inhibitors of porcine 12-LOX provides information for comparison (*5*). These molecules feature a benzene ring para-substituted with a variable-length carboxyalkyl on one side and variable-length alkyl propargyl ether-substituted opposite. With a carboxyalkyl end of fixed length, the contribution to binding from the ether end is approximately −600 cal/methylene for alkyl chains of 6−10 carbons. Longer alkyl chains decreased the level of binding, suggesting a limit to the length of the hydrophobic binding site in this 12-LOX. Adding a methylene on the carboxyalkyl side also decreased the level of binding substantially.

In both SBL1 and cAOS, 5-DSA has greater amplitude of motion at the label site than 8- to 12-DSA. Interaction of a ligand carboxyl with a base is generally featured in discussions of a structure of a ligand−protein complex. Bases available to interact with the carboxyl end of fatty acids have been discussed in reports of X-ray structures of lipoxygenases, and in each case, a lysine or arginine is located near the region that is considered a likely entrance to the internal cavity. Residue Lys260 on helix 2 is near a putative entrance in SBL1, while SBL1 and other lipoxygenases have bases opposite this position in what would correspond to helix 11 in SBL1. The role of Lys260 is uncertain, however, because it has been shown that Lys260Leu has unaltered kinetics (*28*). Perhaps the bulk of the 5-DSA doxyl ring, separated by only three carbons from the carboxylate, interferes with optimal interaction with a base, compared to the situation for 8-, 10-, and 12-DSA. However, given the evident hydrophobic effect in binding thermodynamics of DSA molecules, and the fact that esterified fatty acids are good substrates (*15*, *20*, *29*), a specific charge interaction of the polar end of fatty acids with the protein may be relatively unimportant, or dynamic on the EPR time scale (micro- to nanoseconds), for lipoxygenase substrate or product binding. It is possible that motion of the polar end of a fatty acid between multiple weak binding spots on the surface may assist in driving the hydrocarbon end of the substrate into the nonpolar channel and in repositioning the peroxyl radical catalytic intermediate so that it can reoxidize iron.

This study was designed to provide a spectroscopic approach to examining how fatty acids interact with a binding site on lipoxygenases. The data suggest that the spin-labeled stearates interact with at least part of the substrate site in SBL1. Studies are in progress, using site-directed spin labeling, to determine the location of the DSA spins in relation to defined covalent modification sites by spin−spin interaction and, hence, to identify the entrance to the internal cavity.

ACKNOWLEDGMENT

We thank Gurunathan Laxmikanthan for rendering the images used in Figure 1.

REFERENCES

1. Funk, C. D. (2005) Leukotriene modifiers as potential therapeutics for cardiovascular disease, *Nat. Rev. 4*, 664−672.
2. Serhan, C. N. (2005) Lipoxins and aspirin-triggered 15-epi-lipoxins are the first lipid mediators of endogenous anti-inflammation and resolution, *Prostaglandins, Leukotrienes Essent. Fatty Acids 73*, 141−162.
3. Charlier, C., Henichart, J. P., Durant, F., and Wouters, J. (2006) Structural insights into human 5-lipoxygenase inhibition: Combined ligand-based and target-based approach, *J. Med. Chem. 49*, 186−195.
4. Kenyon, V., Chorny, I., Carvajal, W. J., Holman, T. R., and Jacobson, M. P. (2006) Novel human lipoxygenase inhibitors discovered using virtual screening with homology models, *J. Med. Chem. 49*, 1356−1363.
5. Gorins, G., Kuhnert, L., Johnson, C. R., and Marnett, L. J. (1996) (Carboxyalkyl)benzyl propargyl ethers as selective inhibitors of leukocyte-type 12-lipoxygenases, *J. Med. Chem. 39*, 4871−4878.
6. Bocan, T. M., Rosebury, W. S., Mueller, S. B., Kuchera, S., Welch, K., Daugherty, A., and Cornicelli, J. A. (1998) A specific 15-lipoxygenase inhibitor limits the progression and monocyte-macrophage enrichment of hypercholesterolemia-induced atherosclerosis in the rabbit, *Atherosclerosis 136*, 203−216.
7. Mano, T., Stevens, R. W., Ando, K., Kawai, M., Kawamura, K., Nakao, K., Okumura, Y., Okumura, T., Sakakibara, M., Miyamoto, K., and Tamura, T. (2005) Optimization of imidazole 5-lipoxygenase inhibitors and selection and synthesis of a development candidate, *Chem. Pharm. Bull. 53*, 965−973.
8. Boyington, J. C., Gaffney, B. J., and Amzel, L. M. (1993) The three-dimensional structure of an arachidonic acid 15-lipoxygenase, *Science 260*, 1482−1486.
9. Minor, W., Steczko, J., Stec, B., Otwinowski, Z., Bolin, J. T., Walter, R., and Axelrod, B. (1996) Crystal structure of soybean lipoxygenase L-1 at 1.4 Å resolution, *Biochemistry 35*, 10687−10701.
10. Gilmor, S. A., Villasenor, A., Fletterick, R., Sigal, E., and Browner, M. F. (1997) The structure of mammalian 15-lipoxygenase reveals similarity to the lipases and the determinants of substrate specificity, *Nat. Struct. Biol. 4*, 1003−1009.
11. Skrzypczak-Jankun, E., Amzel, L. M., Kroa, B. A., and Funk, M. O., Jr. (1997) Structure of soybean lipoxygenase L3 and a comparison with its L1 isoenzyme, *Proteins 29*, 15−31.
12. Skrzypczak-Jankun, E., Bross, R. A., Carroll, R. T., Dunham, W. R., and Funk, M. O., Jr. (2001) Three-dimensional structure of a purple lipoxygenase, *J. Am. Chem. Soc. 123*, 10814−10820.
13. Tomchick, D. R., Phan, P., Cymborowski, M., Minor, W., and Holman, T. R. (2001) Structural and functional characterization of second-coordination sphere mutants of soybean lipoxygenase-1, *Biochemistry 40*, 7509−7517.
14. Oldham, M. L., Brash, A. R., and Newcomer, M. E. (2005) Insights from the X-ray crystal structure of coral 8*R*-lipoxygenase, *J. Biol. Chem. 25*, 39545−39552.
15. Gan, Q. F., Browner, M. F., Sloane, D. L., and Sigal, E. (1996) Defining the arachidonic acid binding site of human 15-lipoxygenase. Molecular modeling and mutagenesis, *J. Biol. Chem. 271*, 25412−25418.
16. Borngräber, S., Browner, M., Gillmor, S., Gerth, C., Anton, M., Fletterick, R., and Kuhn, H. (1999) Shape and specificity in mammalian 15-lipoxygenase active site. The functional interplay of sequence determinants for the reaction specificity, *J. Biol. Chem. 274*, 37345−37350.
17. Hornung, E., Walther, M., Kuhn, H., and Feussner, I. (1999) Conversion of cucumber linoleate 13-lipoxygenase to a 9-lipoxygenating species by site-directed mutagenesis, *Proc. Natl. Acad. Sci. U.S.A. 96*, 4192−4197.
18. Knapp, M. J., Seebeck, F. P., and Klinman, J. P. (2001) Steric control of oxygenation regiochemistry in soybean lipoxygenase-1, *J. Am. Chem. Soc. 123*, 2931−2932.
19. Hatcher, E., Soudackov, A. V., and Hammes-Schiffer, S. (2004) Proton-coupled electron transfer in soybean lipoxygenase, *J. Am. Chem. Soc. 126*, 5763−5775.
20. Coffa, G., Imber, A. N., Maguire, B. C., Laxmikanthan, G., Schneider, C., Gaffney, B. J., and Brash, A. R. (2005) On the relationships of substrate orientation, hydrogen abstraction, and product stereochemistry in single and double dioxygenations by soybean lipoxygenase-1 and its Ala542Gly mutant, *J. Biol. Chem. 280*, 38756−38766.

21. Brash, A. R. (1999) Lipoxygenases: Occurrence, functions, catalysis, and acquisition of substrate, *J. Biol. Chem. 274*, 23679−23682.
22. Cheesbrough, T. M., and Axelrod, B. (1983) Determination of the spin state of iron in native and activated soybean lipoxygenase 1 by paramagnetic susceptibility, *Biochemistry 22*, 3837−3840.
23. Klinman, J. P. (2003) Dynamic barriers and tunneling. New views of hydrogen transfer in enzyme reactions, *Pure Appl. Chem. 75*, 601−608.
24. Cristea, M., Engstrom, K., Su, C., Hornsten, L., and Oliw, E. H. (2005) Expression of manganese lipoxygenase in *Pichia pastoris* and site-directed mutagenesis of putative metal ligands, *Arch. Biochem. Biophys. 434*, 201−211.
25. Su, C., and Oliw, E. H. (1998) Manganese lipoxygenase. Purification and characterization, *J. Biol. Chem. 273*, 13072−13079.
26. Coffa, G., and Brash, A. R. (2004) A single active site residue directs oxygenation stereospecificity in lipoxygenases: Stereocontrol is linked to the position of oxygenation, *Proc. Natl. Acad. Sci. U.S.A. 101*, 15579−15584.
27. Prigge, S. T., Boyington, J. C., Gaffney, B. J., and Amzel, L. M. (1996) Structure conservation in lipoxygenases: Structural analysis of soybean lipoxygenase-1 and modeling of human lipoxygenases, *Proteins 24*, 275−291.
28. Ruddat, V. C., Mogul, R., Chorny, I., Chen, C., Perrin, N., Whitman, S., Kenyon, V., Jacobson, M. P., Bernasconi, C. F., and Holman, T. R. (2004) Tryptophan 500 and arginine 707 define product and substrate active site binding in soybean lipoxygenase-1, *Biochemistry 43*, 13063−13071.
29. Brash, A. R., Ingram, C. D., and Harris, T. M. (1987) Analysis of a specific oxygenation reaction of soybean lipoxygenase-1 with fatty acids esterified in phospholipids, *Biochemistry 26*, 5465−5471.
30. Moody, J. S., and Marnett, L. J. (2002) Kinetics of inhibition of leukocyte 12-lipoxygenase by the isoform-specific inhibitor 4-(2-oxapentadeca-4-yne)phenylpropanoic acid, *Biochemistry 41*, 10297−10303.
31. Mitsuda, H., Yasumoto, K., and Yamamoto, A. (1967) Inhibition of lipoxygenase by saturated monohydric alcohols through hydrophobic bondings, *Arch. Biochem. Biophys. 118*, 664−669.
32. Kuninori, T., Nishiyama, J., Shirakawa, M., and Shimoyama, A. (1992) Inhibition of soybean lipoxygenase-1 by normal-alcohols and normal-alkylthiols, *Biochim. Biophys. Acta 1125*, 49−55.
33. Zhu, Z. Y., and Funk, M. O. (1996) Lipoxygenase-1 inhibition with a series of half-product analogs, *Bioorg. Chem. 24*, 95−109.
34. Gaffney, B. J. (1976) The Chemistry of Spin Labels, in *Spin Labeling: Theory and Applications* (Berliner, L. J., Ed.) pp 183−238, Academic Press, New York.
35. Oldham, M. L., Brash, A. R., and Newcomer, M. E. (2005) The structure of coral allene oxide synthase reveals a catalase adapted for metabolism of a fatty acid hydroperoxide, *Proc. Natl. Acad. Sci. U.S.A. 102*, 297−302.
36. Gaffney, B. J., Mavrophilipos, D. V., and Doctor, K. S. (1993) Access of ligands to the ferric center in lipoxygenase-1, *Biophys. J. 64*, 773−783.
37. Wu, F., Katsir, L. J., Seavy, M., and Gaffney, B. J. (2003) Role of radical formation at tyrosine 193 in the allene oxide synthase domain of a lipoxygenase-AOS fusion protein from coral, *Biochemistry 42*, 6871−6880.
38. Mailman, D., and Rose, C. (1990) Binding and solubility of oleic acid to laboratory materials: A possible artifact, *Life Sci. 47*, 1737−1744.
39. Lakshmi, K. V., and Brudvig, G. W. (2000) Electron Paramagnetic Resonance Distance Measurements in Photosynthetic Reaction Centers, in *Distance Measurements in Biological Systems by EPR* (Berliner, L., Eaton, G., and Eaton, S., Eds.) pp 513−567, Kluwer Academic/Plenum Publishers, New York.
40. Rakowsky, M. H., Zecevic, A., Eaton, G. R., and Eaton, S. S. (1998) Determination of high-spin iron(III)-nitroxyl distances in spin-labeled porphyrins by time-domain EPR, *J. Magn. Reson. 131*, 97−110.
41. Nelson, M. J., Cowling, R. A., and Seitz, S. P. (1994) Structural characterization of alkyl and peroxyl radicals in solutions of purple lipoxygenase, *Biochemistry 33*, 4966−4973.
42. Cantor, C. R., and Schimmel, P. R. (1980) *Biophysical Chemistry, Techniques for the Study of Biological Structure and Function*, p 461, W. H. Freeman, New York.
43. Freed, J. H. (1976) Theory of Slow Tumbling ESR Spectra for Nitroxides, in *Spin Labeling: Theory and Applications* (Berliner, L. J., Ed.) pp 53−132, Academic Press, New York.
44. Marsh, D. (1989) Experimental Methods in Spin-Label Spectral Analysis, in *Spin Labeling: Theory and Applications* (Berliner, L. J., and Reuben, J., Eds.) pp 255−303, Plenum Press, New York.
45. Livshits, V. A., and Marsh, D. (2000) Fatty acid binding sites of serum albumin probed by non-linear spin-label EPR, *Biochim. Biophys. Acta 1466*, 350−360.
46. Eaton, S. S., and Eaton, G. R. (2000) Relaxation Times of Organic Radicals and Transition Metal Ions, in *Distance Measurements in Biological Systems by EPR* (Berliner, L. J., Eaton, S. S., and Eaton, G. R., Eds.) pp 29−154, Kluwer Academic/Plenum Publishers, New York.
47. Deligiannakis, Y., and Rutherford, A. W. (1996) Spin−lattice relaxation of the pheophytin, $Pheo^{-}$, radical of photosystem II, *Biochemistry 35*, 11239−11246.
48. Skrzypczak-Jankun, E., Zhou, K., and Jankun, J. (2003) Inhibition of lipoxygenase by (−)-epigallocatechin gallate: X-ray analysis at 2.1 Å reveals degradation of EGCG and shows soybean LOX-3 complex with EGC instead, *Int. J. Mol. Med. 12*, 415−420.
49. Tanford, C. (1973) *The Hydrophobic Effect*, John Wiley & Sons, New York.

BI061415L